

3-16-2017

# Evidence of Erosional Self-Channelization of Pyroclastic Density Currents Revealed by Ground- Penetrating Radar Imaging at Mount St. Helens, Washington (USA)

Andrew C. Gase  
*Boise State University*

Brittany D. Brand  
*Boise State University*

John H. Bradford  
*Boise State University*



This document was originally published in *PloS One* by Public Library of Science. This work is provided under a Creative Commons Attribution 3.0 license. Details regarding the use of this work can be found at: <http://creativecommons.org/licenses/by/3.0/>. doi: 10.1002/2016GL072178

## RESEARCH LETTER

10.1002/2016GL072178

## Key Points:

- A ground-penetrating radar survey at Mount St. Helens reveals two of the largest pyroclastic density current erosion features found to date
- Pyroclastic density currents can erode broad channels capable of confining subsequent flows
- Voluminous erosion by pyroclastic density currents can occur on moderate slopes and in absence of irregular topography

## Supporting Information:

- Supporting Information S1
- Figure S1
- Figure S2
- Figure S3
- Figure S4
- Figure S5
- Figure S6
- Figure S7
- Figure S8
- Figure S9

## Correspondence to:

A. Gase,  
andrewgase@u.boisestate.edu

## Citation:

Gase, A. C., B. D. Brand, and J. H. Bradford (2017), Evidence of erosional self-channelization of pyroclastic density currents revealed by ground-penetrating radar imaging at Mount St. Helens, Washington (USA), *Geophys. Res. Lett.*, *44*, 2220–2228, doi:10.1002/2016GL072178.


Received 1 DEC 2016

Accepted 11 FEB 2017

Accepted article online 16 FEB 2017

Published online 15 MAR 2017

## Evidence of erosional self-channelization of pyroclastic density currents revealed by ground-penetrating radar imaging at Mount St. Helens, Washington (USA)

Andrew C. Gase<sup>1</sup> , Brittany D. Brand<sup>1</sup>, and John H. Bradford<sup>1</sup><sup>1</sup> Department of Geosciences, Boise State University, Boise, Idaho, USA

**Abstract** The causes and effects of erosion are among the least understood aspects of pyroclastic density current (PDC) dynamics. Evidence is especially limited for erosional self-channelization, a process whereby PDCs erode a channel that confines the body of the eroding flow or subsequent flows. We use ground-penetrating radar imaging to trace a large PDC scour and fill from outcrop to its point of inception and discover a second, larger PDC scour and fill. The scours are among the largest PDC erosional features on record, at >200 m wide and at least 500 m long; estimated eroded volumes are on the order of  $10^6$  m<sup>3</sup>. The scours are morphologically similar to incipient channels carved by turbidity currents. Erosion may be promoted by a moderate slope (5–15°), substrate pore pressure retention, and pulses of increased flow energy. These findings are the first direct evidence of erosional self-channelization by PDCs, a phenomenon that may increase flow velocity and runout distance through confinement and substrate erosion.

## 1. Introduction

Pyroclastic density current (PDC) deposits from flows of moderate volume ( $\sim 10^6$  m<sup>3</sup>) are often mantled by intertwined pumice lobes with lateral levees and depressed central channels [e.g., *Wilson and Head*, 1981; *Calder et al.*, 2000]. The morphological similarity of pumice lobes to self-channelized granular flows implies that in certain conditions, PDCs from discrete or waning eruptions can self-channelize [*Jessop et al.*, 2012; *Kokelaar et al.*, 2014]. Self-channelization is commonly observed as levee formation and/or axial erosion (i.e., scouring) in sediment-laden flows, including but not limited to, granular flows [e.g., *Pouliquen et al.*, 1997; *Félix and Thomas*, 2004] and turbidity currents [e.g., *Clark and Pickering*, 1996]. Experimental self-channelized flows have increased runout distance in granular flows [*Kokelaar et al.*, 2014] and increased axial velocity in subaqueous flows [*de Leeuw et al.*, 2016] when compared to nonchannelized flows of equal volume. Therefore, understanding the mechanisms and consequences of PDC self-channelization is critical for hazard prediction.

The role of self-channelization is poorly constrained in sustained, concentrated, fluidized PDCs generated by Plinian column collapse. *Brand et al.* [2014] identify a broad scour and fill feature ( $\sim 300$  m wide;  $\sim 12$  m deep) within the 18 May 1980 PDC deposits at Mount St. Helens (MSH). The scour and fill feature is interpreted as evidence of PDC self-channelization, where PDCs scoured into fresh PDC deposits from earlier phases of the eruption and subsequently deposited within the scour. Yet even well-exposed PDC deposits fail to capture 3-D sedimentary architecture. Constraining the conditions that promoted erosion and the nature of scouring is limited without complementary subsurface imaging.

Our objective is to test whether the scour and fill feature is an expression of sustained, axial erosion and thereby an example of erosional self-channelization or erosion promoted by irregular preflow topography. We use ground-penetrating radar (GPR) to image the scour and fill feature upflow from exposure to the point of inception and to search for subsurface topographic irregularities (e.g., debris avalanche hummocks).

## 2. Geologic Setting

The historic 18 May 1980 MSH eruption began when a massive landslide removed the volcano's upper northern edifice and deposited large hummocks from the break in slope  $\sim 3.5$  km north of the vent to Johnston Ridge and beyond to the west (Figure 1a). The following 9 h eruption generated a Plinian column that began to collapse midday. Numerous column collapse PDCs flowed northward through the breached crater and deposited up to 8 km from the vent (Figure 1a). PDC activity began around 1215 h, waxed to the climactic

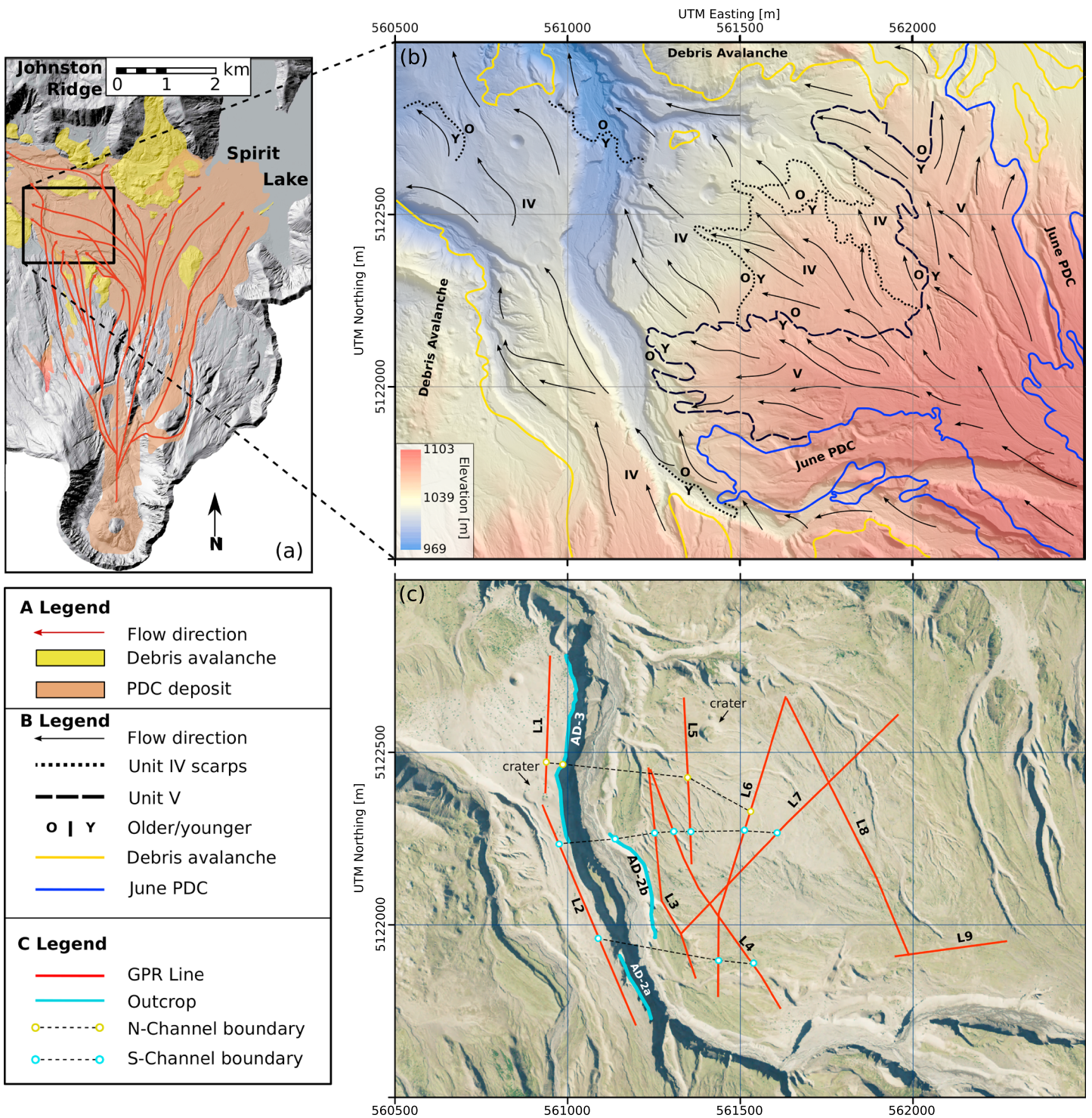


**Figure 1.** Maps of the study site show debris avalanche and PDC deposits and the survey design. Site maps (Figures 1b and 1c) have identical coordinates. (a) Digital elevation model of the northern slope of MSH with debris avalanche hummock locations and major PDC trajectories [Brand et al., 2014]. (b) Combined map of elevation and surficial PDC units from 1980 [Kuntz et al., 1990]. Flow directions are derived from the surface morphology; lower unit flow directions may deviate significantly. (c) Map of GPR lines, outcrops, and subsurface channel boundaries.

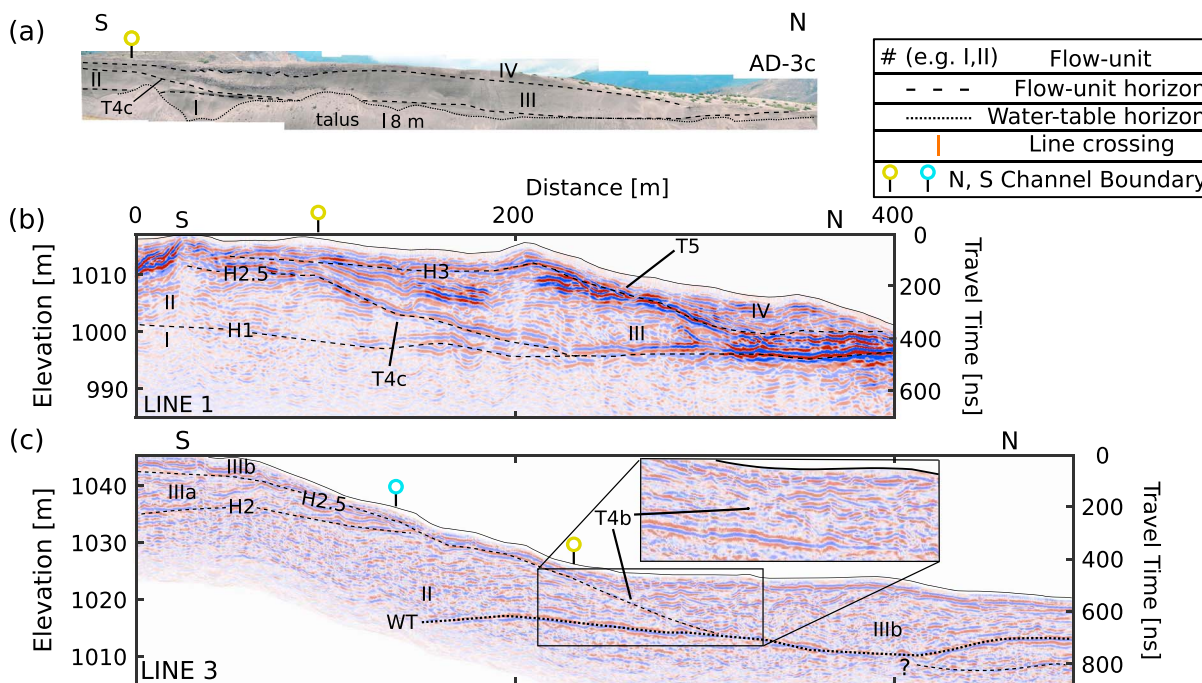


**Figure 2.** Radargram and outcrop locations are shown in Figure 1. Subsections of Figures 2–4 are generally presented in the upflow direction, from northwest to southeast. The scour and fill (a) exposed in outcrop AD-3 is (b) validated in Line 1 and (c) traced upflow. Channel boundaries are defined by the locations of truncation horizons. T4 is the southern boundary of N channel. (Figure 2a) Photograph of outcrop AD-3; 180 m wide. (Figure 2b) Radargram of Line 1. (Figure 2c) Radargram of Line 5. Note the three times vertical length exaggeration on all radargrams.

phase between 1500 and 1715 h, and continued for a short waning phase. PDC deposits in the pumice plain are up to ~40 m thick. Posteruption erosion by the glacier-fed headwaters of the Toutle River exposes tens of kilometers of deposits in the pumice plain.

*Brand et al.* [2014] identify five chronological PDC flow units (Units I–V) deposited by concentrated PDCs capable of retaining elevated pore pressure over the majority of their flow paths. Units I and II, are diffusely stratified to massive and are often capped by ~0.25–0.5 m thick layers of coignimbrite ash. Units III and IV are the most voluminous flow units exposed in the pumice plain. These climactic flow units are often massive with lithic breccias containing both vent and local eroded blocks [Pollock et al., 2016]. The scour and fill feature, introduced above, is found at the Unit II–III flow contact in outcrop AD-3 (Figure 2a). Units III and IV fill the scour and fill feature. The surficial pumice lobe deposits of Unit V correspond to the waning phase of the eruption (Figure 1b).

Our study covers ~2 km<sup>2</sup> of the pumice plain ~5 km northwest of the vent (Figures 1b and 1c). The topography descends regionally to the northwest with a maximum dip of ~15° and total relief of ~125 m. Trajectories derived from the posteruption surface morphology show that PDCs from the waning phase of the eruption followed the northwest topographic gradient [Kuntz et al., 1990] (Figure 1b). Debris avalanche hummocks are clustered along the margins of the site (Figures 1a and 1b) with no exposures upstream from the scour and fill. Our survey is designed to search upflow from the scour and fill for buried debris avalanche hummocks and evidence of PDC erosion.

### 3. Ground-Penetrating Radar Imaging

Data were acquired in common offset mode with a Sensors and Software PulseEKKO Pro GPR. Two sleds with 50 MHz antennas at a fixed offset of 2 m were dragged over the deposit surface. A wheel odometer controlled the 0.5 m trace interval. Simultaneously, we recorded real-time kinematic GPS data for topographic correction. Generally, we could image within Units II–V (~20 m deep). The vertical resolution of 50 MHz electromagnetic waves (i.e., 0.46 m at 0.09 m ns<sup>-1</sup>) is suitable for interpreting flow unit contacts and broad stratigraphic trends.

Processing included time zero correction and band-pass frequency filtering (12–25 to 400–800 MHz). Automatic gain control (AGC) was applied to Line 5, and true amplitude recovery was performed on all other

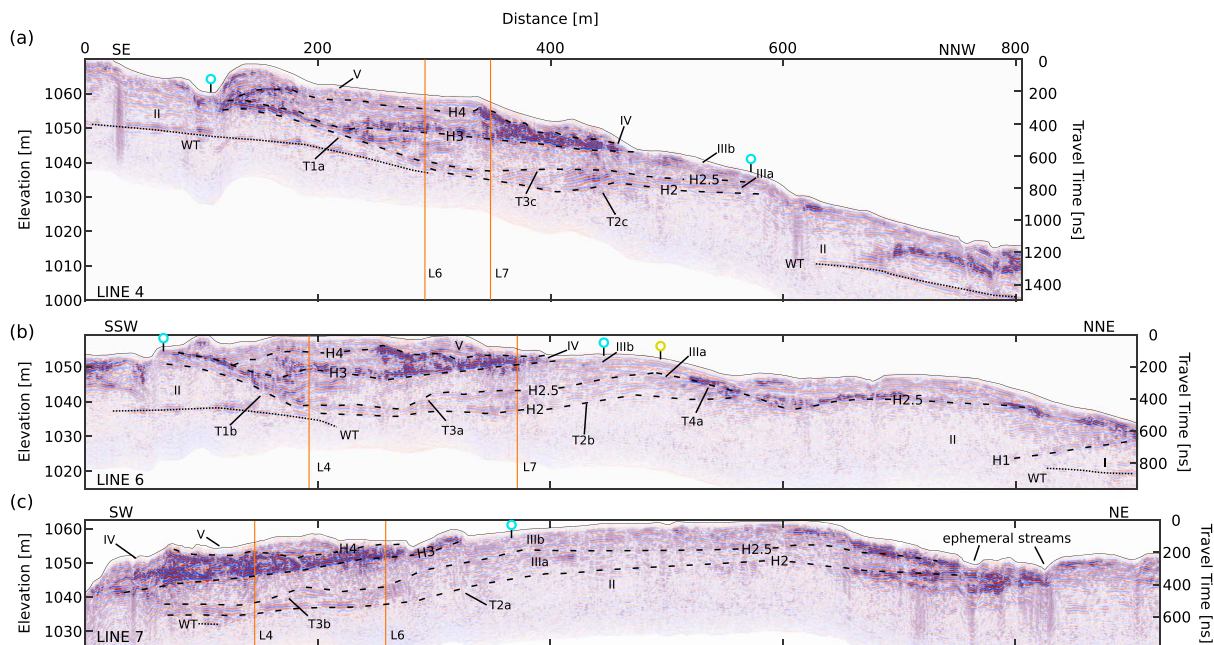


**Figure 3.** Three cross lines show S channel and the point of inception of N channel (exposed scour and fill at outcrop AD-3) between Lines 6 and 7. N channel does not appear in Lines 4 or 7. (a) Radargram of Line 4. (b) Radargram of Line 6. (c) Radargram of Line 7. Line crossings are marked by orange lines.

data. Finally, we migrated the data (frequency-wave number) to collapse diffractions and move dipping reflections to their true subsurface positions then applied topographic correction at  $0.09 \text{ m ns}^{-1}$ . A prior multioffset, reflection tomography GPR survey found  $0.09 \text{ m ns}^{-1}$  to be the average velocity for the MSH pyroclastic deposits [Gase et al., 2015].

## 4. Radargram Descriptions and Interpretations

### 4.1. Description Strategy

We select six key radargrams for their relevance to PDC erosion (Figures 2–4). Unmarked radargrams and radargrams from several other lines that further support our interpretations are available in the supporting information. Reflections are described by their amplitude (i.e., faint or coherent) and geometry (i.e., continuity, shape, and relation to adjacent reflections). Areas of geometrically similar reflectivity are referred to as units. Horizons are referred to as the boundaries of broad areas of similar reflectivity (i.e., units boundaries). In the case that these boundaries result from a geologic boundary (i.e., flow unit boundary) or hydrologic boundary (i.e., water table), a horizon can be a laterally continuous reflection. Horizons are described in stratigraphic order across the entire data set (WT for water table and H1–H5 for lithologic horizons). WT is a strong, laterally continuous reflection that corresponds to the depth of standing water in adjacent streams. Truncation surfaces are segments of horizons that terminate lower reflections. Regionally continuous truncation surfaces traced between radargrams are named by superposition (T1–T5), followed by a lowercase letter corresponding to proximity the vent (*a* is most proximal).

### 4.2. N Channel

To validate the GPR data, we compare the reflectivity of Line 1 with outcrop AD-3 (Figure 2a). The adjacent stream bed is  $\sim 35 \text{ m}$  below the top of the outcrop. Reflections in Line 1 are above the water table and include three horizons that correlate with stratigraphic features in outcrop. The depth and morphology of H1 corresponds to the flow Units I to II contact in outcrop AD-3 (Figure 2a). Above, H2.5 begins to the south at  $\sim 1012 \text{ m}$  elevation, dips northward at  $6^\circ$ , truncates  $\sim 13 \text{ m}$  of lower reflections (T4c), and eventually converges with H1 midline. H3, at  $\sim 3 \text{ m}$  depth to the south, separates lower reflections that are concordant to T4c from near-surface horizontal reflections. To the north, a second truncation surface (T5) terminates Unit III reflections along H3 with relief of  $\sim 12 \text{ m}$ . The wedge of concordant reflections bounded by H2.5 and H3 is morphologically consistent with the dipping and diffuse stratification of Unit III. Horizontal reflections above H3 correspond to Unit IV. Weak midline Unit III reflectivity likely results from scattering by lithic breccias.

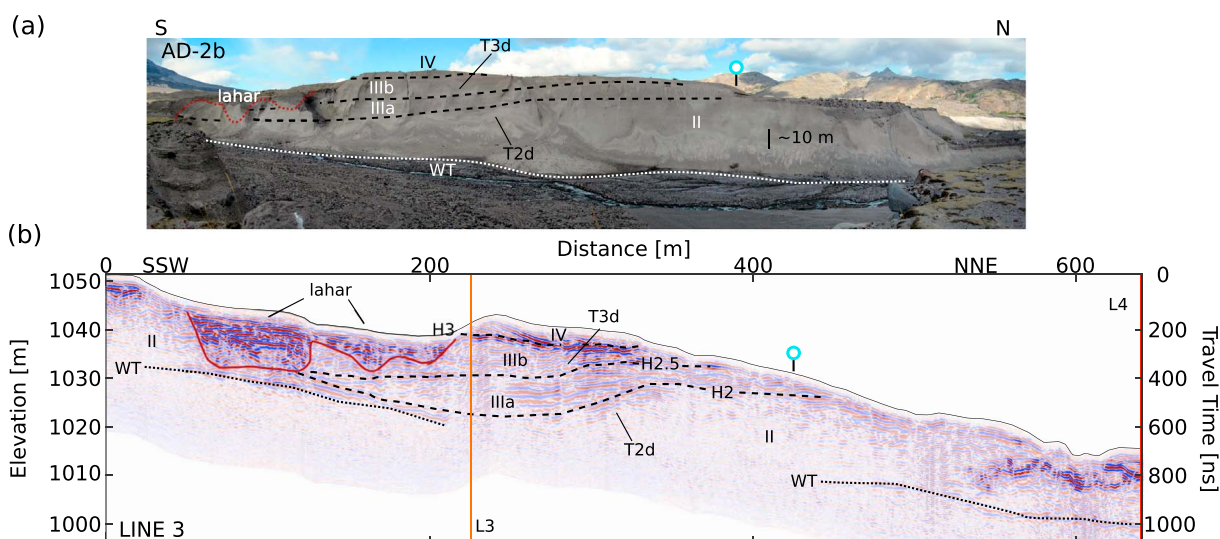


**Figure 4.** S channel is exposed at outcrop AD-2b, where Line 3 is used to correlate reflectivity within Figure 3 to mapped stratigraphy. Lahar erosion to the south obscures the southern boundary of S channel. (a) Panorama of outcrop AD-2b with corresponding flow units. Note that east and west directions are flipped to aid in comparison with all radargrams. (b) Radargram of Line 3.

Our comparison of Line 1 to the exposure demonstrates that GPR can adequately image the scour and fill feature in AD-3 and flow unit contacts.

Line 5 is ~350 m east of outcrop AD-3 (Figures 1c and 2c). Unlike the other lines described herein, Line 5 data were gained with AGC to suppress noise spikes relative to returns from geologic contacts. Water observed in a 7 m deep phreatic crater 50 m to the east (Figure 1c) corroborates WT at 1020 m elevation. Reflections below WT are not accurately interpretable for elevation. At the southern end, H2.5 descends northward at horizontal distance ~150 m, truncates H2, and continues to truncate lower reflections at 7° dip for at least 12 m elevation between horizontal distances 200–300 m (T4b). H2.5 is not visible beneath WT between horizontal distances 300–400 m. A reflection below WT that appears beyond horizontal position 400 m suggests that H2.5 flattens. Along T4b, H2.5 separates lower, discontinuous and sub-parallel reflections from upper, irregular reflections.

Line 6 is east of and slightly oblique to Line 5 (Figure 3a). At the north-northeast end of the line, WT is located ~5 m higher than in Line 5 (Figure 2c). Above WT, the amplitudes of south-dipping reflections increase across H1, which separates Units I and II. H2.5 extends southward to a truncation surface (T4a) that cuts ~10 m of lower reflections at 5.1° dip.

Neither Lines 4 nor 7 (Figure 3a and 3c) contain truncation surfaces that trace to T4. Similarities between T4a in Line 6 (Figure 3b), T4b in Line 5 (Figure 2c), T4c in AD-3 (Figure 2a), and T4c in Line 1 (Figure 2b) in apparent dip, relief, and adjacent radar-facies suggest that they are the same scour and fill feature. We interpret that lower and upper units separated by H2.5 correspond to Units II and IIIb, respectively. Prior to deposition of Unit III, PDCs eroded an asymmetrical channel at least ~0.5 km long that initiated between Lines 6 and 7. This channel (N channel) begins with a northwest trajectory and turns to the west, widens and deepens downflow. The most abrupt increase in erosion occurred between Lines 6 and 7, where the truncation depth jumps from 0 to 10 m. Erosion depth increases by 3 m between Lines 1 and 6.

### 4.3. S Channel

We collected Line 3 alongside outcrop AD-2b (Figure 4) to trace stratigraphy from exposure to Lines 4, 6, and 7 (Figure 3). The adjacent stream is between 15 and 30 m below the top of the outcrop. Lahars eroded channels at the southern half of outcrop AD-2b [Brand *et al.*, 2014]. The Units II to III contact dips ~5° to the south, where Unit III is thickest (~10 m). Unit III is diffusely stratified and separated into subflow units (Units IIIa and IIIb) by a repeated unit contact. A thin lens of Unit IV mantles Unit IIIb.

In Line 3, WT follows the elevation of the adjacent stream (Figure 4b). The unit bounded by WT and H2 corresponds to Unit II in outcrop AD-2b (Figure 4a). At horizontal position ~325 m, lower reflections are truncated by a south dipping portion of H2 (T2d). At horizontal position ~350 m, H2.5 shallowly dips to the south,

truncating Unit IIIa reflections (T3d). Chaotic, high-amplitude reflections at horizontal positions 400–600 m correlate with the lahar deposits and truncate both H2 and H2.5. H3 corresponds to Unit IV (Figure 4a).

Lines 4, 6, and 7 (Figure 3) are described simultaneously, making use of line crossings to correlate horizons from outcrop AD-2b and Line 3 (orange vertical lines in Figures 3 and 4). WT dips slightly to the north in Lines 4 and 6 (Figures 3a and 3b) and remains flat in Line 7 (Figure 3c) before disappearing to the north in all three lines. In the southern ends of Lines 4 and 6 (Figures 3a and 3b), H2 truncates reflections above WT for  $\sim 13$  m at  $10.5^\circ$  dip in Line 6 (T1b) and  $\sim 10$  m at  $3.3^\circ$  dip in Line 4 (T1a). Near the middle of all three lines, the dip of H2 reverses southward to  $3.6^\circ$  in Line 7 (Figure 3c) and  $2.7^\circ$  in Lines 4 and 6 (Figures 3a and 3b), intermittently truncating lower reflections (T2a–T2c). At horizontal positions 175 m in Line 7 (Figure 3c), 250 m in Line 6 (Figure 3b), and 400 m in Line 4 (Figure 3a), H2.5 dips southward and truncates lower, coherent reflections (T3a–T3c). In Line 6 (Figure 3b), H2.5 becomes T4a, separating Units II and IIIb and truncating H2 (T4a). Reflections immediately beneath H2 correspond to Unit II. The coherent and subplanar reflections of the unit beneath H2.5 are attributed to Unit IIIa, as in Line 3 (Figure 4b). Reflections above H2.5 correspond to Unit IIIb.

In Lines 4 and 6 (Figures 3a and 3b), H3 begins to the south at the surface and descends parallel to H2. H3 eventually flattens within the depression bounded by T1 and T2 and dips parallel to T2, meeting the ground surface to the north. In Line 7 (Figure 3c), H3 appears to the south, ascending from 1040 m elevation. Reflections immediately above H3 correspond to Unit IV in outcrop AD-2b and Line 3. H4 marks an upward transition from high- to low-amplitude reflections that roughly parallels the ground surface. We interpret H4 as the Units IV to V contact from the mapped surface of Unit V, a  $\sim 2$ – $3$  m thick pumice lobe deposit that mantles Unit IV (Figure 1b).

We interpret T1 and T2 as the boundaries of a second, unexposed channel complex (hereafter called S channel) formed by multiple phases of erosion and deposition. The west striking truncation boundaries show that Line 6 is closest to a S Channel cross section (Figure 1c). Deep truncation of Unit II reflections by H2 suggests that the current responsible for deposition of Unit IIIa first eroded into Unit II then deposited, resulting in the scour and fill. From superposition along H2.5 and the repeated Unit III subunits between erosion of S channel and N channel, we interpret that S channel formed prior to N channel. The event that eroded N channel coincides stratigraphically with erosion along T3 within S channel. H2.5, H3, and H4 mimic the pooled morphology of H2, and Units IV and V are contained within the area of S channel, suggesting that PDCs flowed through S channel and were partially confined.

## 5. Discussion

Climactic PDCs from the 18 May 1980 eruption of MSH eroded two scour and fill features northwestward across the central pumice plain. The currents responsible for eroding the channels deposited part of their mass within the channels as Units IIIa and IIIb in S channel and Unit IIIb in N channel. The PDC scour and fill features are larger than any previously reported. N channel is  $\sim 12$  m deep,  $>200$  m wide, and at least 500 m long. The larger; S channel is  $\sim 15$  m deep,  $\sim 400$  m wide, and at least 500 m long. From Line 6, the eroded cross-sectional area of S channel is  $\sim 3200$  m<sup>2</sup>. If this area is extended over a half kilometer as the strike lines of S channel suggest (Figure 1c), the total eroded volume is  $\sim 1,600,000$  m<sup>3</sup>. This volume is a small although significant percentage ( $\sim 1.3\%$ ) of the total estimated volume of column collapse PDCs deposited on 18 May 1980 (i.e.,  $\sim 0.12$  km<sup>3</sup>) [Rowley *et al.*, 1981].

Evidence for substrate erosion is recognized in many PDC deposits, yet the causes and consequences of erosion are among the least understood aspects of PDC dynamics [e.g., Dufek, 2016]. Examples of erosion in PDC deposits include amalgamation and shear mixing along flow unit contacts [e.g., Branney and Kokelaar, 2002], identification of accidental components within PDC deposits entrained from upflow exposures [e.g., Buesch, 1992; Calder *et al.*, 2000; Bernard *et al.*, 2014; Brand *et al.*, 2016; Pollock *et al.*, 2016; Roche *et al.*, 2016], reduced thickness of tephra fall deposits underlying PDC deposits [Scarpati and Perrotta, 2012], and channel-like scours carved into the substrate [e.g., Fisher, 1977; Kieffer and Sturtevant, 1988; Sparks *et al.*, 1997; Cole *et al.*, 1998; Brown and Branney, 2004; Brand and Clarke, 2009; Brand *et al.*, 2014]. Fluidized and dry granular flow experiments demonstrate that erosion can be aided by vertical pore pressure gradients [Roche *et al.*, 2013] and/or by shear at the flow base [Rowley *et al.*, 2011]. Field observations suggest that erosive capacity is also affected by topographic conditions that increase shear or collisional stresses including the following: (1) propagation on steep slopes close to the substrate's angle of repose ( $>25^\circ$ ) [Cole *et al.*, 1998; Bernard *et al.*, 2014;

*Brand et al.*, 2016]; (2) transitions from high to low slope [*Scarpati and Perrotta*, 2012]; (3) irregular topography, such as debris avalanche hummocks [*Pollock et al.*, 2016]; or (4) channelized terrains, such as gullies along the flanks of volcanoes [*Sparks et al.*, 1997; *Cole et al.*, 1998].

No radargrams or outcrops show evidence of pre-PDC irregular topography (i.e., buried debris avalanche hummocks or bedrock) that could channelize or disrupt PDCs to initiate erosion of the channels. Both S and N channels begin where PDCs turned from northward to northwestward and where the slope began to increase from 5° to ~12–15° for N channel and ~10–15° for S channel. The increase from shallow to moderate slope may have influenced the location and initiation of erosion. Both channels are asymmetric, unexpectedly displaying greater erosional relief on their southern boundaries. This asymmetry implies that (1) the PDCs propagated oblique to the topographic gradient and were partially confined by the northwest facing slope, (2) more complete erosion occurred at the northern boundary, or (3) that flows began turning north at the location of our survey.

Erosion may be aided by the air retention of the substrate. *Brand et al.* [2014] provide evidence for the retention of gas between pore spaces after the PDCs came to rest, including the following: (1) soft sediment deformation due to loading of lithic blocks over finer-grained deposits; (2) a high proportion of fines in the deposits, which would have reduced deposit permeability and gas escape; (3) lack of distinct, well-developed grain fabric (typical of granular flow), even in the distal regions, suggesting interstitial gas buffered particle-particle interactions at the time of deposition; and (4) numerous secondary PDCs, which occurred along slopes of ~5–6° [*Kuntz et al.*, 1990], reflecting high pore pressure within the primary PDC deposits. Experimental studies of fluidized granular flows demonstrate that the head of a flow generates underpressure that can be responsible for erosion via an upward pressure gradient [e.g., *Roche*, 2012; *Roche et al.*, 2013]. Elevated pore pressure in the substrate could increase erosion by strengthening the upward pressure gradient at the base of the PDCs. We suspect that an aerated substrate is also more susceptible to erosion via shear due to decreased friction between grains, thereby allowing substrate erosion on relatively shallow slopes (~5–15°).

It is also possible that the currents' internal conditions promoted erosion. Erosion occurs through the combined effects of basal stress imparted by the PDC that acts to mobilize the substrate and the weak mechanical resistance of an unconsolidated and aerated substrate at a moderate slope angle (5–15°). The state of the PDCs (i.e., flow regime, velocity, and concentration) is influenced by conditions at the vent, within the eruption column, and along the path of transport. Pulses of increased flux at the vent could produce PDCs with greater erosive capacity that coincide with flow unit contacts. All truncation horizons discussed herein occur immediately before deposition of climactic flow units. Thus, it is likely that the currents responsible for eroding S and N channels were more energetic than PDCs produced earlier in the eruption.

Our findings demonstrate that during sustained, waxing and waning eruptions that produce PDCs for several hours, cycles of deposition and erosion by PDCs modify the terrain encountered by subsequent flows [e.g., *Cole et al.*, 1998]. The erosional process may be similar to seafloor erosion by turbidity currents that produces extensive submarine channels off continental shelves. Turbidity currents self-channelize either by lateral deposition of levees that constrict flows and promote downstream scouring [*de Leeuw et al.*, 2016] or from broad scours that elongate and deepen through repeated passage of turbidity currents [*Fildani et al.*, 2013]. The channels reported herein are morphologically similar to the incipient scours or broad megafaults excavated from a single to few erosive flows [e.g., *Elliott*, 2000; *Fildani et al.*, 2013] rather than the mature, sinuous, hundreds of kilometers long and hundreds of meters deep submarine canyons produced by numerous flows over many years [cf. *Clark and Pickering*, 1996].

Turbidity currents with thicknesses between 1.3 and 5 times the channel depth are considered quasi-channelized, in which the fast-moving basal portion of the current is channelized while the overlying unconfined middle to top portion of the current is unconfined [*Mohrig and Buttles*, 2007]. Lateral spreading is suppressed in quasi-channelized currents, thereby preserving an axial zone of high flow energy. In our study, increased thicknesses of Units IIIa and IIIb within the channel axes suggest partial channelization of the PDCs responsible for their deposition. Repeated erosion and deposition of Unit III within the S channel boundary further demonstrates that the current responsible for eroding a channel can also deposit part of its mass within the channel. Units IV and V are contained within S channel, suggesting a transition from quasi-channelization of PDCs that deposited Unit IIIb, to more complete channelization of the PDCs responsible for Units IV and V as the volume of the PDCs waned and the channel filled. Thus, our evidence suggests that the dimensions of the scours were sufficient to partially channelize subsequent PDCs.



It is not possible to determine the effects of erosional self-channelization on the velocity and runout distance of PDCs from our data. However, the combination of field, numerical, and experimental results provide insight into the influence of self-channelization on velocity and runout distance. *Brand et al.* [2014] note an increase in the size and concentration of accidental blocks within N channel relative to outside N channel, suggesting increased carrying capacity in partially channelized flows. Simulations of PDCs propagating down slopes show that flows confined to sinuous or straight channels have increased flow velocity and runout distance relative to the same flow conditions propagating across a smooth slope [Dufek, 2016]. Dynamically scaled turbidity current experiments reveal increased longitudinal flow velocities along the axis of confined flows, even in particularly shallow channels [de Leeuw et al., 2016]. Based on these previous works, we hypothesize that erosionally self-channelized PDCs exhibit increased flow runout distance and/or longitudinal velocity.

## 6. Conclusion

GPR imaging at MSH reveals the largest PDC scour and fill features reported to date, suggesting that concentrated, sustained PDCs are capable of erosional self-channelization. The channels discovered herein demonstrate that (1) PDCs from eruptions sustained for several hours can produce large scours that alter topography and channelize subsequent flows in a manner analogous to incipient channels in submarine turbidity currents and (2) a moderate topographic gradient, substrate properties, such as partial fluidization of fresh PDC deposits, and energetic pulses may facilitate substrate erosion. However, which variables have primary controls on erosion and the influence of self-channelization on flow mobility and runout distance remain unclear. Future experimental and modeling efforts that investigate the causes and effects of erosional self-channelization would improve our understanding of volcanic hazards.

### Acknowledgments

We thank Nicholas Pollock, Tate Meehan, Travis Nielson, Darin Schwartz, and Alexander Miller for their generous assistance with data acquisition. This study was improved through peer review by Sarah Kruse and Olivier Roche, as well as informal review by Nicholas Pollock and Lee Liberty. The Boise State Center for Geophysical Investigation of the Shallow Subsurface (CGISS) provided all geophysical equipment. This work was partially supported by a National Science Foundation grant (NSF-EAR 0948588) and a Geological Society of America graduate student research grant. Radargrams without interpretations are available in the supporting information. Raw and processed data are archived at <http://cgiss.boisestate.edu/data-downloads/>.

### References

- Bernard, J., K. Kelfoun, J. L. Le Pennec, and S. V. Vargas (2014), Pyroclastic flow erosion and bulking processes: Comparing field-based vs. modeling results at Tungurahua volcano, Ecuador, *Bull. Volcanol.*, *76*(9), 858, doi:10.1007/s00445-014-0858-y.
- Brand, B. D., and A. B. Clarke (2009), The architecture, eruptive history, and evolution of the Table Rock Complex, Oregon: From a Surtseyan to an energetic maar eruption, *J. Volcanol. Geotherm. Res.*, *180*(2), 203–224, doi:10.1016/j.jvolgeores.2008.10.011.
- Brand, B. D., C. Mackaman-Lofland, N. M. Pollock, S. Bendaña, B. Dawson, and P. Wichgers (2014), Dynamics of pyroclastic density currents: Conditions that promote substrate erosion and self-channelization—Mount St Helens, Washington (USA), *J. Volcanol. Geotherm. Res.*, *276*, 189–214, doi:10.1016/j.jvolgeores.2014.01.007.
- Brand, B. D., S. Bendaña, S. Self, and N. Pollock (2016), Topographic controls on pyroclastic density current dynamics: Insight from 18 May 1980 deposits at Mount St. Helens, Washington (USA), *J. Volcanol. Geotherm. Res.*, *321*, 1–17, doi:10.1016/j.jvolgeores.2016.04.018.
- Branney, M. J., and B. P. Kokelaar (2002), *Pyroclastic Density Currents and the Sedimentation of Ignimbrites*, *Geol. Soc. of London Mem.*, vol. 27, Geol. Soc. of London, U. K.
- Brown, R. J., and M. J. Branney (2004), Bypassing and diachronous deposition from density currents: Evidence from a giant regressive bed form in the Poris ignimbrite, Tenerife, Canary Islands, *Geology*, *32*(5), 445–448, doi:10.1130/G20188.1.
- Buesch, D. C. (1992), Incorporation and redistribution of locally derived lithic fragments within a pyroclastic flow, *Geol. Soc. Am. Bull.*, *104*(9), 1193–1207, doi:10.1130/0016-7606.
- Calder, E. S., R. S. J. Sparks, and M. C. Gardeweg (2000), Erosion, transport and segregation of pumice and lithic clasts in pyroclastic flows inferred from ignimbrite at Lascar Volcano, Chile, *J. Volcanol. Geotherm. Res.*, *104*(1–4), 201–235, doi:10.1016/S0377-0273(00)00207-9.
- Clark, J. D., and K. T. Pickering (1996), *Submarine Channels: Processes and Architecture*, 231 pp., Vallis Press, London.
- Cole, P. D., E. S. Calder, T. H. Druitt, R. Hoblitt, R. Robertson, R. S. J. Sparks, and S. R. Young (1998), Pyroclastic flows generated by gravitational instability of the 1996–97 lava dome of Soufriere Hills volcano, Monserrat, *Geophys. Res. Lett.*, *25*(18), 3425–3428.
- de Leeuw, J., J. T. Eggenhuisen, and M. J. Cartigny (2016), Morphodynamics of submarine channel inception revealed by new experimental approach, *Nat. Commun.*, *7*, 10886, doi:10.1038/ncomms10886.
- Dufek, J. (2016), The fluid mechanics of pyroclastic density currents, *Annu. Rev. Fluid Mech.*, *48*(1), 459–485, doi:10.1146/annurev-fluid-122414-034252.
- Elliott, T. (2000), Megaflute erosion surfaces and the initiation of turbidite channels, *Geology*, *28*(2), 119–122, doi:10.1130/0091-7613(2000)28<119:MESATI>2.0.CO;2.
- Félix, G., and N. Thomas (2004), Relation between dry granular flow regimes and morphology of deposits: Formation of levees in pyroclastic deposits, *Earth Planet. Sci. Lett.*, *221*(1), 197–213, doi:10.1016/S0012-821X(04)00111-6.
- Fildani, A., S. M. Hubbard, J. A. Covault, K. L. Maier, B. W. Romans, M. Traer, and J. C. Rowland (2013), Erosion at inception of deep-sea channels, *Mar. Pet. Geol.*, *41*, 48–61, doi:10.1016/j.marpetgeo.2012.03.006.
- Fisher, R. V. (1977), Erosion by volcanic base-surge density currents: U-shaped channels, *Geol. Soc. Am. Bull.*, *88*(9), 1287–1297, doi:10.1130/0016-7606(1977)88<1287:EBVBDC>2.0.CO;2.
- Gase, A., J. H. Bradford, and B. D. Brand (2015), Ground penetrating radar and active seismic investigation of stratigraphically verified pyroclastic deposits. Abstract NS41A-1916 presented at 2015 Fall Meeting, AGU, San Francisco, Calif., 14–18 Dec.
- Jessop, D. E., K. Kelfoun, P. Labazuy, A. Mangeny, O. Roche, J. L. Tillier, and G. Thibault (2012), LiDAR derived morphology of the 1993 Lascar pyroclastic flow deposits, and implication for flow dynamics and rheology, *J. Volcanol. Geotherm. Res.*, *245*, 81–97, doi:10.1016/j.jvolgeores.2012.06.030.
- Kieffer, S. W., and B. Sturtevant (1988), Erosional furrows formed during the lateral blast at Mount St. Helens, May 18, 1980, *J. Geophys. Res.*, *93*(B12), 14,793–14,816, doi:10.1029/JB093iB12p14793.
- Kokelaar, B. P., R. L. Graham, J. M. N. T. Gray, and J. W. Vallance (2014), Fine-grained linings of leveed channels facilitate runout of granular flows, *Earth Planet. Sci. Lett.*, *385*, 172–180, doi:10.1016/j.epsl.2013.10.043.

- Kuntz, M. A., P. D. Rowley, and N. S. MacLeod, (1990), Geologic map of pyroclastic-flow and related deposits of the 1980 eruptions of Mount St. Helens, Washington, U.S. Geol. Surv. Misc. Geol. Invest. Map I-1950, U.S. Geol. Surv., Reston, Va.
- Mohrig, D., and J. Buttles (2007), Deep turbidity currents in shallow channels, *Geology*, *35*(2), 155–158, doi:10.1130/G22716A.1.
- Pollock, N. M., B. D. Brand, and O. Roche (2016), The controls and consequences of substrate entrainment by pyroclastic density currents at Mount St Helens, Washington (USA), *J. Volcanol. Geotherm. Res.*, *325*, 135–147, doi:10.1016/j.jvolgeores.2016.06.012.
- Pouliquen, O., J. Delour, and S. B. Savage (1997), Fingering in granular flows, *Nature*, *386*, 816–817, doi:10.1038/386816a0.
- Roche, O. (2012), Depositional processes and gas pore pressure in pyroclastic flows: An experimental perspective, *Bull. Volcanol.*, *74*(8), 1807–1820, doi:10.1007/s00445-012-0639-4.
- Roche, O., Y. Niño, A. Mangeney, B. Brand, N. Pollock, and G. A. Valentine (2013), Dynamic pore-pressure variations induce substrate erosion by pyroclastic flows, *Geology*, *41*(10), 1107–1110, doi:10.1130/G34668.1.
- Roche, O., D. C. Buesch, and G. A. Valentine (2016), Slow-moving and far-travelled dense pyroclastic flows during the Peach Spring super-eruption, *Nat. Commun.*, *7*, 10890, doi:10.1038/ncomms10890.
- Rowley, P. D., M. A. Kuntz, and N. S. MacLeod (1981), Pyroclastic-flow deposits, *U.S. Geol. Surv. Prof. Pap.*, *1250*, 489–512.
- Rowley, P. J., P. Kokelaar, M. Menzies, and D. Waltham (2011), Shear-derived mixing in dense granular flows, *J. Sediment. Res.*, *81*, 874–884, doi:10.2110/jsr.2011.72.
- Scarpati, C., and A. Perrotta (2012), Erosional characteristics and behavior of large pyroclastic density currents, *Geology*, *40*(11), 1035–1038, doi:10.1130/G33380.1.
- Sparks, R. S. J., M. C. Gardeweg, E. S. Calder, and S. J. Matthews (1997), Erosion by pyroclastic flows on Lascar Volcano, Chile, *Bull. Volcanol.*, *58*(7), 557–565, doi:10.1007/s004450050162.
- Wilson, L., and J. W. Head (1981), Morphology and rheology of pyroclastic flows and their deposits, and guidelines for future observations, *U.S. Geol. Surv. Bull.*, *1250*, 513–524.